J Solid State Electrochem (2012) 16:2667–2674
DOI 10.1007/s10008-012-1689-4

ORIGINAL PAPER

Nickel oxide/expanded graphite nanocomposite electrodes for supercapacitor application

Juan Xu · Xiaofang Gu · Jianyu Cao · Wenchang Wang · Zhidong Chen

Received: 11 December 2011 / Revised: 2 February 2012 / Accepted: 13 February 2012 / Published online: 28 February 2012

Abstract Nickel oxide/expanded graphite (NiO/EG) nanocomposites with different loading of EG were prepared through chemically depositing $Ni(OH)_2$ in EG followed by thermal annealing and characterized by scanning electron microscopy (SEM), powder X-ray diffraction (XRD), Brunauer–Emmet–Teller (BET) isotherm and electrochemical measurements. The prepared NiO/EG composites were found to be crystalline and highly porous with high specific surface area and pore volume. SEM analysis reveals uniform porous morphology for NiO in the NiO/EG-60 nanocomposites which shows good specific capacitance (510 $F g^{-1}$) at a current density of 100 mA g^{-1} in 6 mol L^{-1} KOH measured by chronopotentiometry employing a three-electrode system. The specific capacitance retention of the NiO/EG-60 nanocomposites was found to be ca. 95% after 500 continuous galvanostatic charge–discharge cycles, indicating that the NiO/EG nanocomposites can become promising electroactive materials for supercapacitor application.

Keywords Nickel oxide/expanded graphite (NiO/EG) nanocomposites · Supercapacitors · Chemical deposition

J. Xu · X. Gu · J. Cao · W. Wang · Z. Chen
Changzhou University,
Changzhou 213164, People's Republic of China

J. Xu · Z. Chen (✉)
Jiangsu Sola Materials and Technology Key Laboratory,
Changzhou 213164, People's Republic of China
e-mail: cjytion3@163.com

Introduction

Supercapacitors, combining the features of high specific power density, fast charge–discharge rate, and long cycle life, have occupied the area between batteries and conventional capacitors and are recognized as vital electrical energy storage devices [1]. Based on different energy storage mechanism, supercapacitors are classified into two categories: (1) electric double layer capacitors (EDLCs), resulting from charge separation at the electrode/electrolyte interface and (2) electrochemical pseudocapacitors (EPCs), arising from fast and reversible faradic redox reactions that occur within the electro-active materials [2]. Among the various electroactive materials used for EPCs electrode, amorphous hydrated RuO_2 formed by cathodic electrodeposition method has been identified to be an influential material because of its fairly high specific capacitance (786 $F g^{-1}$), good electronic conductivity and excellent cyclability [3]. However, the commercial application of RuO_2 was hindered by its high cost and toxicity. Hence, considerable efforts have been devoted to develop inexpensive alternative electrode materials having good capacitive characteristics with long cycle life time and excellent reversibility, such as transition metal oxide, metal hydroxides, polymeric materials, and so on [4–6].

With its low cost, environmental friendly nature, high theoretical capacitance (2,584 $F g^{-1}$ within 0.5 V), and easy preparation, nickel oxide (NiO) has drawn extensive research attention and been considered as a promising pseudocapacitive material in alkaline electrolyte [7]. Unfortunately, NiO is a p-type semiconductor with low conductivity and slow rate of redox interconversion in NiO bulk materials [8]. While a number of chemical methods such as sol–gel [9],

potentiodynamic [10], hard templating [11, 12], hydrothermal [13], microwave [14], and precipitation [15] methods have been employed to prepare high-performance NiO nanomaterial, its practical specific capacitance reported previously is still unsatisfactory because of its low utilization and high resistance, which has resulted in high polarization and thus, limited its practical application to supercapacitors. For this reason, many efforts have dedicated to enhance the electrochemical utilization and conductivity of NiO by distributing it in diverse high conductive and specific surface area nanomaterials for the development of next-generation supercapacitors [7, 16–24]. For example, supercapacitors constructed of NiO/carbon nanotube composites have been reported with specific capacitances of 160, 523, 1,000, and 1,329 $F g^{-1}$ at their respective discharge current density [7, 16–18]. A specific capacitance 581 $F g^{-1}$ for NiO/ordered mesoporous carbon composites was reached by a combination of incipient wetness impregnation and hydrothermal method [19]. NiO also can be loaded into activated-carbon and show an increased specific capacitance of 194 $F g^{-1}$ [20]. Tao et al. prepared NiO/SiNW composite thin film by chemical etching followed by electroless plating method and attained a specific capacitance of 681 $F g^{-1}$ [21]. Liu et al. reported that the specific capacitance of NiO/RuO_2 composite electrode can approximate to 210 $F g^{-1}$ at a current density of 5 mA cm^{-2} [22]. Porous NiO/Ag composite film synthesized by a combination process of chemical bath deposition and silver mirror reaction can exhibit a specific capacitance of 330 $F g^{-1}$ at 2 $A g^{-1}$ [8]. By using a simple thermal decomposition process, Deng et al., successfully prepared Ni-CoO_x nanocomposite, which shows a maximum specific capacitance of 287 $F g^{-1}$ at a current density of 0.2 A g^{-1} [23]. Flower-like NiO/TiO_2 nanocomposites prepared by an electrode-position-oxidation and thermal dehydration process exhibited an improved specific capacitance of 46.3 mF cm^{-2} [24]. The specific capacitance of graphene-supported NiO prepared by electrophoretic deposition and chemical deposition method can reach 400 and 525 $F g^{-1}$ [25–28].

Recently, expanded graphite (EG) has been widely investigated in the scientific community because of its unique properties in terms of excellent electrical conductivity, high porosity, large specific surface area, cheap price, and good chemical stability and related new application as a energy generation and storage material in EDLCs [29], alcohol fuel cell [30], and an active electrode material in electrochemical sensor [31]. Furthermore, we in our early reports found that electrode materials with a rich porous structure and large active surface area will provide a very short diffusion pathway for electrolyte ions to efficiently contact more electroactive sites for faradic energy storage, even at high current densities, leading to enhanced electrochemical properties [12, 32]. In this context, loading NiO into EG is expected to provide a chance to improve the electrochemical performance of NiO for EPCs.

Experimental

Preparation of EG

EG was prepared from flake graphite through oxidation reaction and transitory high temperature treatment [33]. Briefly, graphite, concentrated nitric acid, phosphoric acid, and potassium permanganate were thoroughly mixed together at a mass ratio of 1:5.6:20:0.25 at 300 K under continuous stirring. After being filtrated, this product was washed exhaustively with distilled water and dried at 380 K for 2 h. Expansion of the above product was performed in a temperature programmed oven at 1,200 K for 30 s.

Synthesis of NiO/EG nanocomposites

Homogeneous chemical precipitation is a simple and effective method to control and obtain desired product. NiO was loaded into the above-prepared EG using a chemical precipitation process followed by thermal annealing. First, 0.0747 g EG was uniformly dispersed in 20 ml of 0.2 M $NiCl_2$ solution by sonication for 2 h to get a homogeneous suspension. Then, 25 ml of 0.4 M NaOH was drop-wise added into the above mixture under vigorous stirring at 0 °C to produce nickel hydroxide ($Ni(OH)_2$) from the chloride. After centrifugation and washing with distilled water, the resultant $Ni(OH)_2$/EG precipitate was dried in vacuum at 60 °C for 12 h and then calcined in N_2 atmosphere at 400 °C for 2 h, which was followed by naturally cooling to room temperature. The as-prepared final NiO/EG nanocomposites sample is denoted as NiO/EG-20, which represents that the weight percentage of EG in the above-prepared NiO/EG nanocomposite is 20 wt.%. Other NiO/EG-40, NiO/EG-60, NiO/EG-80, and bare NiO samples were fabricated according to the same procedures, respectively. The as-prepared NiO/EG nanocomposite sample was heated at 800 °C in air, and EG is burn off for all samples after 50 h. Based on the mass loss of the NiO/EG nanocomposite samples, the content of EG in nanocomposites can be estimated.

Structure and morphology characterization

To obtain the information on the crystal structure and morphology for the resulting NiO/EG nanocomposite, X-ray powder diffraction (XRD) measurement was carried out on a powder diffraction system (XRD, Rigaku D/max 2500 PC) using Cu Kα radiation. The morphology of the samples was observed

by scanning electron microscopy (SEM, JSM-6360LA). Surface area and porosity of the samples were obtained from N_2 adsorption-desorption isotherm and Barret–Joyner–Halenda (BJH) plots (Micromeritics porosimeter ASAP 2010).

Electrode preparation and electrochemical characterization

For electrochemical characterization, NiO/EG nanocomposite electrodes were prepared according to the following steps. Typically, 90 wt.% NiO/EG nanocomposites powder, 5 wt.% acetylene black as a conducting agent and 5 wt.% polytetrafluorethylene as a binder were homogeneously mixed and pressed into a nickel foam (1×1 cm) current collector under a pressure of 8 MPa.

Electrochemical measurements in a three electrode system were carried out at room temperature consisting of the NiO/EG nanocomposites electrode as working electrode, a saturated calomel electrode (SCE; $Hg/HgCl_2$) as reference electrode, and a platinum plate (1×1 cm) as counter electrode. The used electrolyte was 6 M KOH solution.

For good estimation of electrode materials, a hybrid electrochemical capacitor with active carbon (AC) electrode (1×1 cm) as negative electrode was designed. The NiO/EG-60 nanocomposites cathode and AC anode were pressed together and separated by a porous nonwoven cloth separator. The mass of NiO/EG-60 nanocomposites and AC were 20 and 60 mg.

The electrochemical behavior of the NiO/EG nanocomposites electrode was characterized by cyclic voltammetry (CV), galvanostatic charge–discharge tests and electrochemical impedance spectroscopy (EIS) at VersaSTAT3 electrochemical workstation (Princeton Applied Research, USA). The CV was conducted in a potential range between −0.1 and 0.50 V versus SCE at various scan rates. The constant current charge–discharge tests were carried out at different currents within a potential range of 0–0.4 V. EIS was carried out at open circuit potential in 6 M KOH with a frequency range of 0.01 to 10^5 Hz.

Results and discussion

Morphology and structure analysis

To investigate the surface morphology of different NiO/EG nanocomposites as prepared by simple chemical precipitation, SEM images are shown in Fig. 1. The surface of bare EG is quite smooth, and bare NiO nanoparticles are prone to aggregate into large secondary particles. After the addition of EG, uniform particle-shaped NiO can be uniformly and fully coated on the surface of EG. Similar morphology was also reported by Shornikova et al. using electrochemical method [34]. Moreover, with the increasing addition of EG, the size of NiO in the NiO/EG nanocomposites become finer, which may be attributed to the increase of defective sites and addition of oxygen-containing functional groups on carbon surface [35, 36]. Since bare EG has much higher conductivity than bare NiO [37, 38], it is expected that the

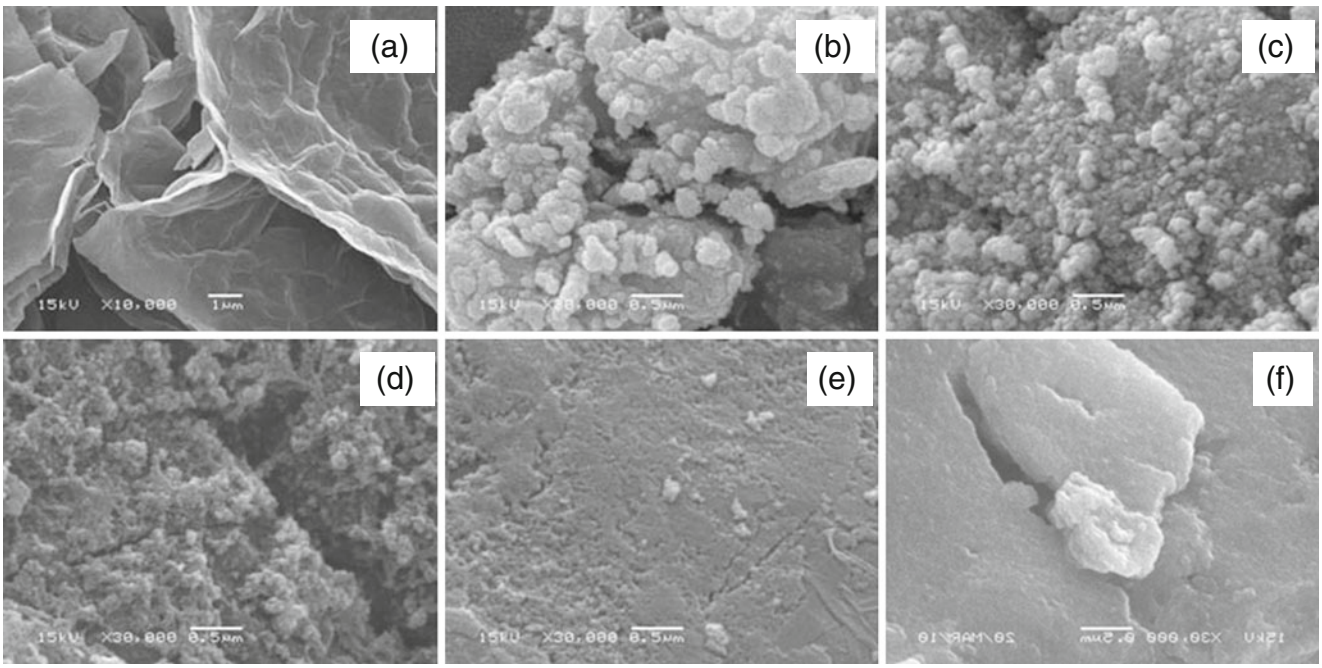

Fig. 1 SEM images of bare EG (**a**), bare NiO (**b**), NiO/EG-20 (**c**), NiO/EG-40 (**d**), NiO/EG-60 (**e**), and NiO/EG-80 (**f**) nanocomposites

NiO/EG nanocomposite may reveal better electrochemical performance than bare NiO.

The powder XRD patterns of the NiO-loaded EG nanocomposites prepared in our experiment are shown in Fig. 2. For comparison, the bare NiO and EG are also listed. The bare NiO and NiO/EG nanocomposites clearly show three typical NiO characteristic diffraction peaks at 2θ values of 36.9° (111), 42.8° (200), and 62.4° (220), which is in agreement with that of the standard values (JCPDS card no. 14-0117). The bare EG peaks are also clearly seen at 26.4° (002) and 54.50° (004) in the NiO/EG nanocomposites. Furthermore, compared with bare NiO, the characteristic peaks of NiO in the NiO/EG nanocomposites broaden, indicating that the particle size of NiO in the NiO/EG nanocomposites is smaller than that of bare NiO, which can provide higher specific surface area and more active sites for faradic redox reaction of the NiO. In the light of the XRD peak widths and Scherrer equation [39], the crystallite sizes of NiO in the bare NiO, NiO/EG-20, NiO/EG-40, NiO/EG-60, and NiO/EG-80 nanocomposites are respectively estimated to be about 28.5, 17.7, 10.0, 7.3, and 6.4 nm.

High surface area and suitable porosity are crucial factors for the specific capacitance value of NiO [12]. Important structural parameters of NiO/EG nanocomposites are derived from their respective N_2 adsorption-desorption isotherms (not shown here) and tabulated in Table 1. From Table 1, we found that with the increase in the EG amount, the Brunauer–Emmet–Teller (BET) specific surface areas of the NiO/EG nanocomposites are slightly decreased, but the BJH pore sizes are gradually boosted. The reason lies in that the BET surface area of EG is 48 $m^2\ g^{-1}$, largely lower than that of pure NiO. Considering the BET surface of the EG and the weight ratio of EG, the actual specific surface of NiO in the NiO/EG nanocomposites increase with the gradual addition of EG. On the other hand, suitable pore size of the NiO/EG nanocomposites can make the accessibility of OH^- ions with electro-active materials easy and high, which is very important for their high capacitance behavior. We presume that the increase in BJH pore size and NiO specific surface is favorable to enhance the electrochemical activity of NiO nanostructures.

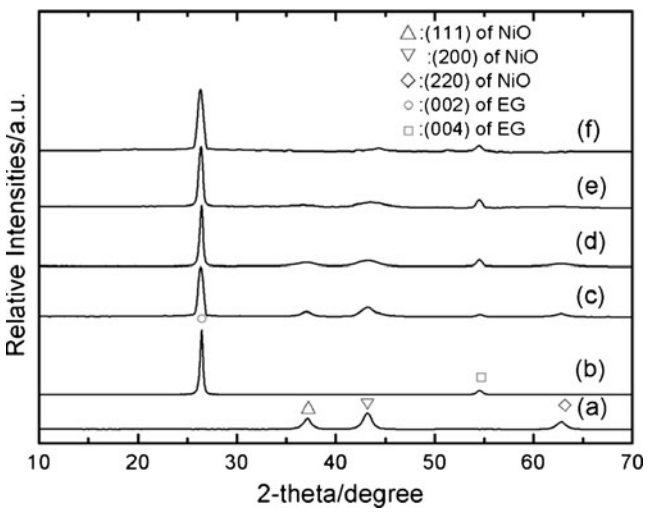

Fig. 2 XRD profiles of bare NiO (*a*), bare EG (*b*), NiO/EG-20 (*c*), NiO/EG-40 (*d*), NiO/EG-60 (*e*), and NiO/EG-80 (*f*) nanocomposites

Electrochemical characterization

CV curves of different NiO/EG nanocomposites were performed at a scan rate of 2 mV s^{-1} in 6 M KOH electrolyte to examine their electrochemical properties. As shown in Fig. 3, a couple of well-defined broad redox reaction peaks have been observed within the potential range from −0.1 to 0.5 V (versus SCE) for each NiO/EG nanocomposite, revealing that electrochemical capacity of NiO mainly originates from fast and quasi-reversible faradic reaction. According to literatures [13, 40], the anodic peak is for the oxidation process of NiO to NiOOH, and the cathodic peak derive from its reverse procedure. At the same scan rate, the electrochemical specific capacitances are proportionate to the graphical integration area of CV curves [7, 41]. Comparing the curves of the NiO/EG nanocomposites and bare NiO, it can be inferred that NiO/EG nanocomposites have higher specific capacitance than bare NiO, and the value of NiO/EG-60 nanocomposite can reach maximum. Furthermore, with the increase in EG amount, the redox reaction peak potential difference of the NiO/EG nanocomposites decrease. The CV curves of bare NiO and NiO/EG-60 nanocomposites electrodes at 500 mV s^{-1} were shown in the inset, which manifest that the NiO/EG-60 nanocomposite electrode has higher current and lesser redox peak potential difference than bare NiO. These phenomenon can be interpreted in terms of that adding EG to NiO can improve the dispersion of NiO on the surface of EG and provide a lot of superficial electro-active species to take part in faradic redox reaction, so as to enhance the electrochemical conductivity, reversibility and utilization of NiO. Moreover, the NiO/EG nanocomposite has larger pore size than bare NiO, which can ease the access of electrolyte ions to reaction sites and faster ion transfer inside the pore structure. So, compared with bare

Table 1 Structural parameters of the samples

Samples	BET surface area ($m^2\ g^{-1}$)	BJH pore volume ($cm^3\ g^{-1}$)	BJH pore diameter (nm)
NiO	175	0.12	20.1
NiO/EG-20	163	0.10	27.7
NiO/EG-40	151	0.12	33.5
NiO/EG-60	151	0.15	35.4
NiO/EG-80	145	0.14	35.2
EG	48	0.15	10.4

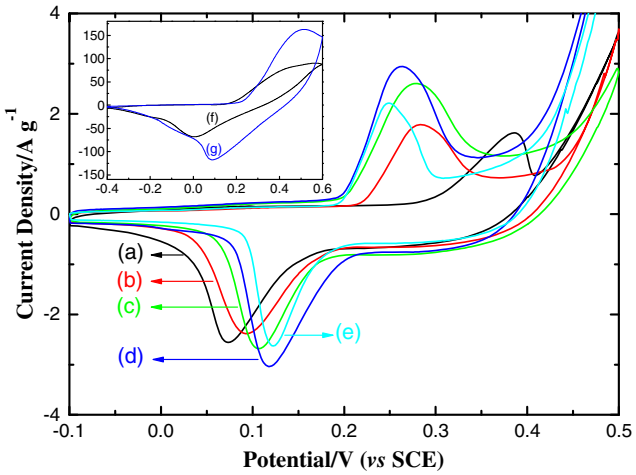

Fig. 3 Cyclic voltammograms of bare NiO (*a*), NiO/EG-20 (*b*), NiO/EG-40 (*c*), NiO/EG-60 (*d*), and NiO/EG-80 (*e*) nanocomposites electrodes at a scan rate of 2 mV s^{-1} in 6 mol L^{-1} KOH aqueous solution. The *inset* is the CV curves of bare NiO (*f*) and NiO/EG-60 nanocomposites (*g*) electrodes at 500 mV s^{-1}

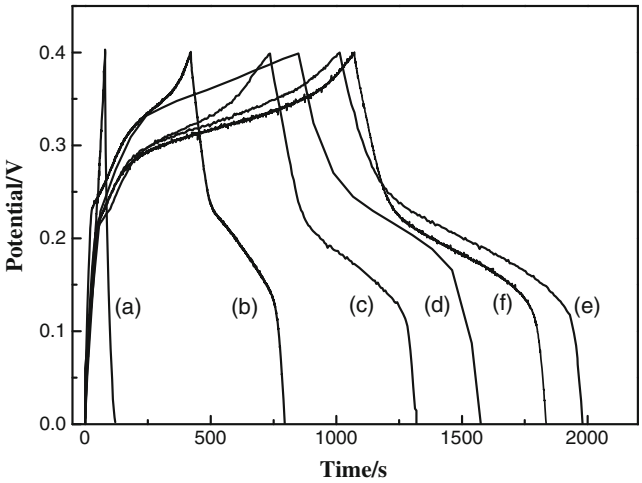

Fig. 5 Charge–discharge curves of EG (*a*), NiO (*b*), NiO/EG-20 (*c*), NiO/EG-40 (*d*), NiO/EG-60 (*e*), and NiO/EG-80 (*f*) nanocomposites electrodes at 200 mA g^{-1}

NiO, NiO in the NiO/EG nanocomposite has faster, more reversible faradic reaction and higher electrochemical utilization.

Figure 4 presents the CV curves of the NiO/EG-60 nanocomposite electrode measured at different scan rates in 6 M KOH. The anodic and cathodic peak current densities are 1.44 and −1.51 Ag^{-1} (scan rate, 1 mV s^{-1}), 2.96 and −3.01 Ag^{-1} (scan rate, 2 mV s^{-1}), 4.27 and −4.41 Ag^{-1} (scan rate, 3 mV s^{-1}), 5.69 and −5.78 Ag^{-1} (scan rate, 4 mV s^{-1}), 7.02 and −7.15 Ag^{-1} (scan rate, 5 mV s^{-1}), respectively. The anodic peak current densities are almost symmetric to their corresponding cathodic peak current densities, suggesting good reversibility of fast charge–discharge response. The proximate linear relationship of the peak current density versus the scan rate (inset in Fig. 4) demonstrates high-power property [7].

To further evaluate the electrochemical capacity of the synthesized NiO/EG composites, we used these composites to fabricate electrodes for supercapacitors and characterized them with chronopotentiometric measurements. Galvanostatic charge–discharge experiment are conducted at different current densities to find out the specific capacitance values and stability of the NiO/EG nanocomposite electrode. For NiO/EG nanocomposite, all the charge–discharge curves are non-linear, clearly manifesting their pseudocapacitance behavior, as presented in Figs. 5 and 6. The specific capacity of as-prepared samples can be calculated using the following equation [42]: $C=(I\times\Delta t)/(m\times\Delta V)$. Where C (in F g^{-1}) represents the specific capacitance, I (A) is the galvanostatic current used for charge/discharge, Δt (s) is the time elapsed for the

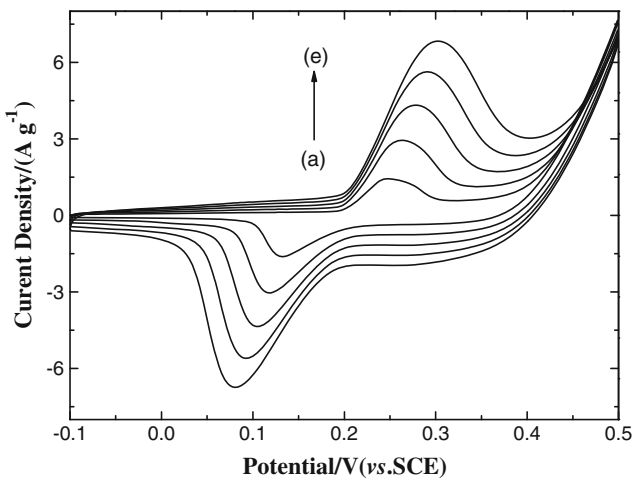

Fig. 4 CV curves of NiO/EG-60 nanocomposite electrode at different sweep rates of 1 (*a*), 2 (*b*), 3 (*c*), 4 (*d*), and 5 (*e*) mV s^{-1}

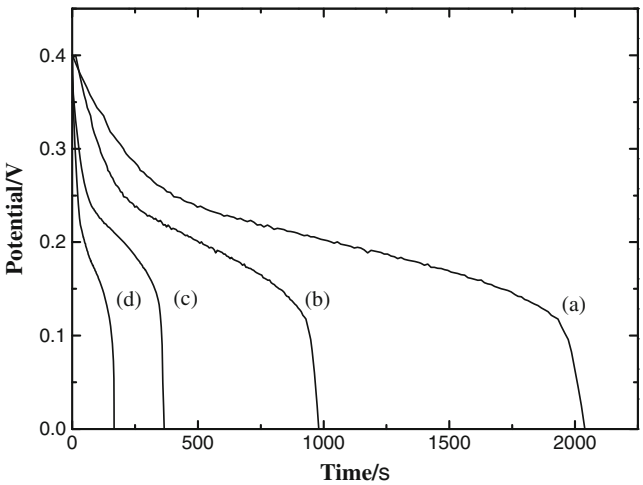

Fig. 6 Discharge curves of NiO/EG-60 nanocomposites electrode at 100 (*a*), 200 (*b*), 500 (*c*), and 1,000 (*d*) mA g^{-1}

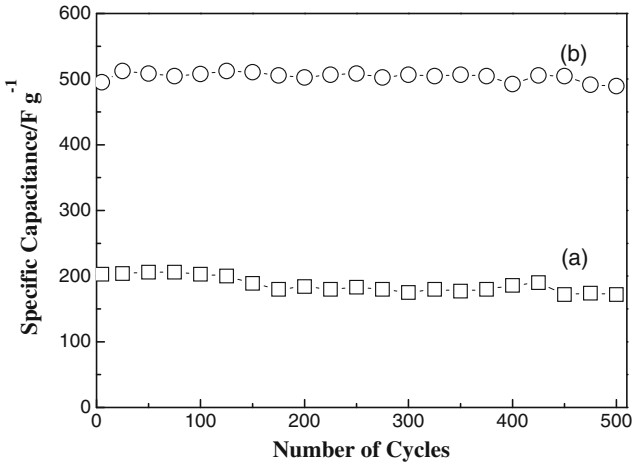

Fig. 7 Cycle-life plot of bare NiO (*a*) and NiO/EG-60 composite (*b*) electrode at a current density of 100 mA g^{-1} in 6 M KOH

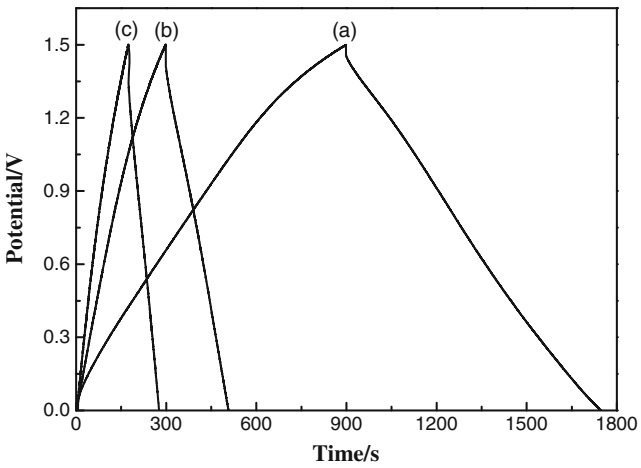

Fig. 9 Charge–discharge curves of AC-NiO/EG-60 composite hybrid supercapacitors at 5 (*a*), 15 (*b*), and 25 (*c*) mA cm^{-2}

discharge cycle, ΔV (V) is the discharge voltage interval, and *m* (g) is the weight of NiO/EG nanocomposite within the electrode. As calculated from Fig. 5, the specific capacitances of EG, NiO, NiO/EG-20, NiO/EG-40, NiO/EG-60, and NiO/EG-80 are 24, 189, 299, 365, 486, and 428 F g^{-1} at a discharge current density of 200 mA g^{-1}, respectively, demonstrating that the specific capacitance of the EG supported nanosize NiO is strongly dependent on their dispersion and surface area. Our research on EG shows that its capacity is about 24 F g^{-1} in 6 M KOH; hence, we can deduce that the capacitive behaviors of these composites are mainly attributed to the pseudocapacitance of NiO. The NiO/EG-60 nanocomposite electrode shows a high specific capacitance of 486 F g^{-1}, indicating that the electrochemical utilization of the NiO in the NiO/EG nanocomposite electrode was higher than that of the bare NiO. The outstanding electrochemical capacitance of the synthesized NiO/EG-60 composite electrode can be attributed to its suitable pore size and large specific surface area, which help to enlarge the contact area between electrode and electrolyte and improve the surface adsorption-desorption process of alkali cations. Owing to low specific capacitance of bare EG (24 F g^{-1}) and high weight percentage of EG in the NiO/EG-80 nanocomposite electrode, its specific capacitance is lower than that of the NiO/EG-60 nanocomposite electrode.

It is critical for supercapacitors to maintain large capacitances under high charge–discharge current densities because of the high power demand from commercial electric vehicles. Figure 6 shows the galvanostatic discharge curves of the NiO/EG-60 nanocomposites electrode in 6 mol L^{-1} KOH electrolyte at various current densities. The specific capacitances of the NiO/EG-60 nanocomposites calculated from each discharge curve attain 510, 486, 458, and 416 F g^{-1} by applying the discharge current densities of 100, 200, 500, and

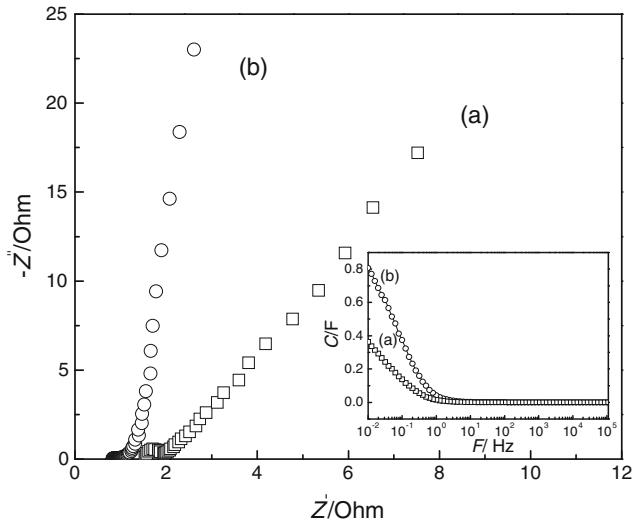

Fig. 8 Nyquist plots of bare NiO (*a*) and NiO/EG-60 composite (*b*) electrodes. The *inset* is the frequency dependence of the real part of the capacitance for bare NiO (*a*) and NiO/EG-60 composite (*b*)

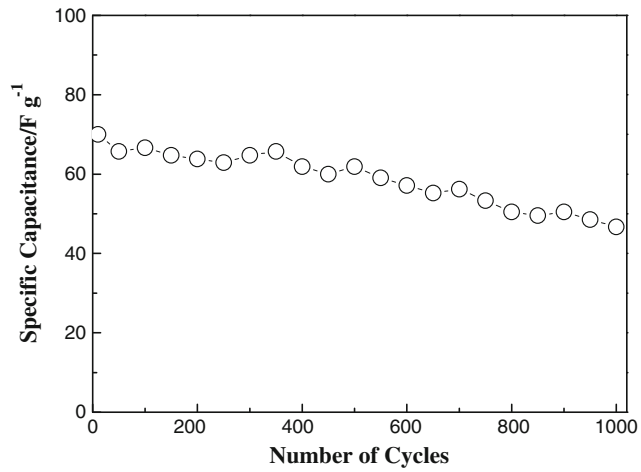

Fig. 10 Cycling profile of the AC-NiO/EG-60 composite hybrid supercapacitors at a current of 25 mA cm^{-2}

1,000 mA g^{-1}, respectively. Importantly, compared with its specific capacitance at 100 mA g^{-1}, the value of the NiO/EG-60 nanocomposites electrode at 1,000 mA g^{-1} only decreases by 18.5%. The small capacitance fading at a very high galvanostatic current density shows that EG supported NiO allows for a rapid redox reaction at high current densities. Due to the comparatively slow rate of redox reactions at high current densities, the specific capacitance decreases with increasing current density [43]. At low discharge current densities, voltage drop (IR) is negligible, and both outer and inner pore surfaces can be effectively utilized for electrolyte propagation and redox reaction, which contribute to achieve high specific capacitance. However, at high discharge current densities, IR losses become significant, and inner region of the pore cannot be accessed by OH^- ions.

Figure 7 displays the charge–discharge stability and galvanostatic cycling life of NiO/EG-60 nanocomposites at a current density of 200 mA g^{-1} in 6 mol L^{-1} KOH. It is found that the NiO/EG-60 nanocomposite electrode exhibited good stability and reversibility with cycling efficiency of 95% after 500 cycles.

The electrical resistances, which were correlated to the microstructure and electrochemical properties of the NiO/EG-60 nanocomposite electrodes, are characterized by EIS measurements between 0.01 and 10^5 Hz, as shown in Fig. 8. The Nyquist plot consists of a semicircle at high frequency region and a straight line at low frequency region. From the point intersecting with the real axis in the range of high frequency, the internal resistance of the bare NiO and NiO/EG-60 electrode in an open circuit condition is evaluated to be ca. 1.6 and 0.9 Ω, which is a combination of ionic resistance of electrolyte, intrinsic resistance of the electro-active material, and contact resistance between the active material and the current collector [44]. In the high-to-medium frequency region, one semicircle related to faradic redox processes can be discovered, which should be considered as the charge transfer resistance at the electrode/electrolyte interface [45]. Furthermore, the charge transfer resistance of NiO/EG-60 electrode is lower than that of bare NiO. The linear part at lower frequency corresponds to the diffusive resistance of the OH^- ion, named Warburg impedance, but the phase angle for the impedance plot of the NiO/EG-60 electrode was observed to be higher than 45° in the low frequencies. This deviation is attributed to easy access of the OH^- ion with the electro-active NiO/EG-60 nanocomposite electrode and reversible faradic redox reaction, implying that the unique structure and composition of the NiO/EG-60 nanocomposite electrode can facilitate OH^- ion diffusion and electron transfer in solid electrode. The higher the slope of the diffusion line, the lower the capacitor's diffusive resistance [11]. Hence, the NiO/EG-60 nanocomposite electrode has lower charge transfer resistance and diffusion resistance than bare NiO electrode, reflecting higher specific capacitance.

Figure 9 displays the charge–discharge curves of the AC-NiO/EG-60 composite hybrid supercapacitors at 5, 15, and 25 mA cm^{-2}. The specific capacitances of the AC-NiO/EG-60 composite hybrid supercapacitors calculated from each discharge curve reach 81, 74, and 70 $F g^{-1}$, respectively.

The galvanostatic cycling profile of the AC-NiO/EG-60 composite hybrid supercapacitors at a current of 25 mA cm^{-2} was presented in Fig. 10. After 1,000 cycles, the specific capacitance of the AC-NiO/EG-60 composite hybrid supercapacitors can attain 46 $F g^{-1}$.

Conclusions

This work examined the morphology, structure and capacitive properties of EG substrate supported NiO via a chemical precipitation method followed by heat treatment in air at 400 °C for 2 h. SEM analysis indicated that electro-active NiO was uniformly coated on the surface of EG, constructing a rough and nanoporous structure. In comparison to the bare NiO, the NiO/EG composite showed higher specific capacitance and electrochemical reversibility. Electrochemical measurements indicated that the NiO/EG-60 composite electrode exhibited a good rate capability and presented an excellent cycle life in 6 M KOH, which were attributed to its appropriate morphology and structure characteristics. The excellent electrochemical performance coupled with the low cost and simple preparation process render NiO/EG-60 composite electrode very promising for practical application in supercapacitors.

Acknowledgments The authors gratefully acknowledge financial support from the National Science Foundation of China (21003015 and 21103014), the Science Foundation of Jiangsu Province (BE201113 and 2011Z0062), the Science Foundation of Changzhou (CJ20115020), and the Priority Academic Program Development (PAPD) of Jiangsu Higher Education Institutions.

References

1. Aricò AS, Bruce P, Scrosati B, Tarascon JM, Schalkwijk WV (2005) Nat Mater 4:366–377
2. Zhang Y, Feng H, Wu X, Wang L, Zhang A, Xia T, Dong H, Li X, Zhang L (2009) Int J Hydrogen Energy 34:4889–4899
3. Zheng YZ, Ding HY, Zhang ML (2008) Thin Solid Films 516:7381–7385
4. Gao Y, Chen S, Cao D, Wang G, Yin J (2010) J Power Sources 195:1757–1760
5. Abdolmohammad-Zadeh H, Rezvani Z, Sadeghi GH, Zorufi E (2011) Anal Chim Acta 685:212–219
6. Snook GA, Kao P, Best AS (2011) J Power Sources 196:1–12
7. Nam KW, Lee ES, Kim JH, Lee YH, Kim KB (2005) J Electrochem Soc 152:A2123–A2129
8. Wu JB, Li ZG, Lin Y (2011) Electrochim Acta 56:2116–2121
9. Cheng J, Cao GP, Yang YS (2006) J Power Sources 159:734–741
10. Prasad KR, Miura N (2004) Appl Phys Lett 85:4199–4201

11. Jiao F, Hill AH, Harrison A, Berko A, Chadwick AV, Bruce PG (2008) J Am Chem Soc 130:5262–5266
12. Xu J, Gao L, Cao JY, Wang WC, Chen ZD (2010) Electrochim Acta 56:732–736
13. Meher SK, Justin P, Rao GR (2010) Electrochim Acta 55:8388–8396
14. Cao CY, Guo W, Cui ZM, Song WG, Cai W (2011) J Mater Chem 21:3204–3209
15. Inamdar AI, Kim YS, Pawar SM, Kim JH, Im H, Kim H (2011) J Power Sources 196:2393–2397
16. Lee JY, Liang K, An KH, Lee YH (2005) Synth Met 150:153–157
17. Lin P, She Q, Hong B, Liu X, Shi Y, Shi Z, Zheng M, Dong Q (2010) J Electrochem Soc 157:A818–A823
18. Gao B, Yuan CZ, Su LH, Chen L, Zhang XG (2009) J Solid State Electrochem 13:1251–1257
19. Feng J, Zhao J, Tang B, Liu P, Xu J (2010) J Solid State Chem 183:2932–2936
20. Yuan GH, Jiang ZH, Aramata A, Gao YZ (2005) Carbon 43:2913–2917
21. Tao B, Zhang J, Miao F, Hui S, Wan L (2010) Electrochim Acta 55:5258–5262
22. Liu XM, Zhang XG (2004) Electrochim Acta 49:229–232
23. Deng JJ, Deng JC, Liu ZL, Deng HR, Liu B (2009) J Mater Sci 44:2828–2835
24. Xie Y, Huang C, Zhou L, Liu Y, Huang H (2009) Compos Sci Techn 69:2108–2114
25. Xia X, Tu J, Mai Y, Chen R, Wang X, Gu C, Zhao X (2011) Chem Eur J 17:10898–10905
26. Kottegoda IRM, Idris NH, Lu L, Wang JZ, Liu HK (2011) Electrochim Acta 56:5815–5822
27. Ji Z, Wu J, Shen X, Zhou H, Xi H (2011) J Mater Sci 46:1190–1195
28. Zhao B, Song J, Liu P, Xu W, Fang T, Jiao Z, Zhang H, Jiang Y (2011) J Mater Chem 21:18792–18798
29. Ka BH, Oh SM (2008) J Electrochem Soc 155:A685–A692
30. Bhattacharya A, Hazra A, Chatterjee S, Sen P, Laha S, Basumallick I (2004) J Power Sources 136:208–210
31. Krawczyk P, Skowroński JM (2010) J Appl Electrochem 40:91–98
32. Xu J, Gao L, Cao J, Wang W, Chen Z (2011) J Solid State Electrochem 15:2005–2011
33. Li J, Da H, Liu Q, Liu S (2006) Mater Lett 60:3927–3930
34. Shornikova ON, Sorokina NE, Avdeev VV (2007) Inorg Mater 43:938–944
35. Azadi P, Farnood R, Meier E (2010) J Phys Chem A 114:3962–3968
36. Afanasov IM, Shornikova ON, Avdeev VV, Lebedev OI, Tendeloo GV, Matveev AT (2009) Carbon 47:513–518
37. Dhakate SR, Mathur RB, Sharma S, Borah M, Dhami TL (2009) Energy Fuel 23:934–941
38. Raut BT, Pawar SG, Chougule MA, Sen S, Patil VB (2011) J Alloys Compd 509:9065–9070
39. Wu MS, Huang YA, Yang CH (2008) J Electrochem Soc 11:A798–A805
40. Zhao DD, Bao SJ, Zhou WJ, Li HL (2007) Electrochem Commun 9:869–874
41. Shen C, Wang X, Zhang W, Kang F (2011) J Power Sources 196:10465–10471
42. Liu XM, Zhang XG, Fu SY (2006) Mater Res Bull 41:620–627
43. Morishita T, Soneda Y, Hatori H, Inagaki M (2007) Electrochim Acta 52:2478–2484
44. Luo JM, Gao B, Zhang XG (2008) Mater Res Bull 43:1119–1125
45. Yuan A, Zhang Q (2006) Electrochem Commun 8:1173–1178